Results in Engineering 22 (2024) 102247

Contents lists available at ScienceDirect

Results in Engineering

journal homepage: www.sciencedirect.com/journal/results-in-engineering

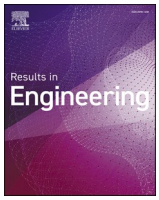

Dynamic model and robust control for the PEM fuel cell systems

Jie Ying Tan, Raja Mohd Taufika Raja Ismail *, Mohd Shawal Jadin

Faculty of Electrical and Electronics Engineering Technology, Universiti Malaysia Pahang Al-Sultan Abdullah, 26600 Pekan, Pahang, Malaysia

ARTICLE INFO

Keywords:
PEM fuel cell
Super-twisting sliding mode
Floating interleaved boost converter
MPPT

ABSTRACT

In response to the escalating challenges posed by climate change, the global energy sector has witnessed a paradigm shift towards sustainable alternatives. The promising fuel cell technology known as the proton exchange membrane fuel cell (PEMFC) has found widespread use in a variety of mobile and stationary applications. This paper presents a super-twisting sliding mode (STSM) control for maximum power point tracking (MPPT) on the proton exchange membrane fuel cell (PEMFC) system incorporated floating interleaved boost converter (FIBC). This work aims to extract the maximum power from the PEMFC by means of robust control in conjunction with FIBC to improve current ripple. The proposed controller is designed for the PEMFC system by combining the STSM and MPPT methods. The designed MPPT control tracks down the maximum power point of the system, and the corresponding current values act as the reference values for the STSM controller. The results show that incorporating the PEMFC with the FIBC can result in current ripple reduction when compared with a traditional interleaved boost converter (IBC). The obtained results demonstrate the capability of the PEMFC closed-loop control system to maintain the system's robustness under fuel cell parameter variations.

1. Introduction

The environmental crisis has become a concern for people all over the world. From the environmental perspective, the main reason that caused the climate change and pollution problem is the use of fossil fuels as energy production in many applications. Therefore, clean and green energy becomes core to dealing with the inescapable reduction of fossil fuels [1–3]. Sustainable energy like solar, wind, geothermal, biomass and fuel have been used to supersede the fossil fuel which caused the pollution issue [4–6]. Hydrogen fuel cells are a type of renewable energy that can produce energy by converting chemical elements into electricity without involving the combustion of fuel [7,8]. Thus, hydrogen fuel cell energy is regarded as one of the most promising power generators offering clean energy and system robustness [9,10]. Hydrogen energy can help to reduce carbon emission in the atmosphere since the ways to make hydrogen is either carbon-free or significantly less demand on carbon [11,12]. After the pandemic, countries are working hard to meet their Sustainable Development Goals (SDGs). Hydrogen fuel cell energy has been essential in achieving this goal. Hydrogen energy can always be related to Goal-7 of the SDGs, which is affordable and clean energy. Several studies have been done to find the links between SDG and the hydrogen economy. There is a research study that claimed that hydrogen energy is a game-changer and how the hydrogen economy can help in the success to achieve Goal-7 [13]. The government of India wants to increase its renewable energy capacity to 500 GW by 2030 and get 50 % of its energy from renewable sources, which is in line with SDG-7. The main goal of SDG-7 is to make clean, modern energy affordable for every family by 2030 and to double the rate of energy efficiency improvement around the world. Hence, it showed that many countries had taking action in achieving SDG-7 and hydrogen energy will surely be a main part of this achievement [14,15].

Since a single fuel cell produces such a low voltage, stacks of fuel cells are usually connected in series to boost the voltage level. The fuel cell's output voltage will be significantly affected by the load requirement due to the fuel cell's non-linear voltage-ampere properties. To get the required output voltage, a DC/DC converter must be applied in between the fuel cell stack and the DC load [16]. For mobile and stationary applications, PEMFC fuel cells are the preferred technology. This is primarily due to its zero-pollutant fuel, low operating temperature, and great power efficiency [17]. According to the results of some experiments, PEMFC systems work better and last longer when operated at their maximum power point (MPP) [18]. However, internal and external variables influence the fuel cell device's efficiency. Internal factor is the cell flooding and membrane break conditions. External factors are the external features that will have an indirect effect on the fuel cell system's durability. Overshoot and undershooting in a fuel cell system and ripples

* Corresponding author.
E-mail address: rajamohd@umpsa.edu.my (R.M.T. Raja Ismail).

https://doi.org/10.1016/j.rineng.2024.102247
Received 7 December 2023; Received in revised form 24 April 2024; Accepted 8 May 2024
Available online 9 May 2024

in the current and load changes are all external variables [19].

Numerous studies have shown an increase in efficiency by combining the power converter with the fuel cell technology. Due to the fuel cell stack's low voltage, a power converter must be connected to the system to guarantee adequate energy conversion from the system to the load. Therefore, a power converter interfaces the fuel cell stack and the load bus. Many applications and systems use power converters like buck converters, boost converters, buck-boost converters, and DC-link voltage regulators [20–22]. However, the IBC is getting more attention from researchers because of its advantages compared with other power converters. Inhibition of voltage and current ripples is one of the primary benefits of the IBC, which contributes to the system's longevity [23,24]. However, the IBC provides the same voltage step-up ratio as the boost converter. Therefore, many researchers have researched the other type of converters with lower voltage stress based on the interleaved boost converter structure. The FIBC is a type of boost converter that has been the subject of extensive study due to its high voltage gain and low voltage stress characteristics. It can achieve the same voltage gain at a more appropriate duty cycle [25]. The power converter will usually be implemented into a mathematical model as a dynamic system based on its circuit structure to adapt well to the control theories in various applications.

Nevertheless, many control methods have been implemented in the PEMFC system and the results are discussed in terms of various aspects. Classical linear control like PI and PID control is commonly used when designing the DC/DC converter. However, the PEMFC system's non-linear properties mean that linear management approaches cannot handle disturbances and uncertainties. Recent research and discussion in the PEMFC system have focused on non-linear control methods such as Fuzzy Logic Controller (FLC) [26], Data-driven Method [27], Particle Swarm Optimization (PSO) [28] and Sliding Mode Control (SMC) [29,30]. The PEMFC method frequently employs the use of SMC. Because of its high system robustness [31], and in particular because of its advantages in minimizing the chattering effect that happens with traditional SMC, the STSM controller has gained a lot of attention in recent years. The non-linear SMC is applied to an IBC and PEMFC system to increase system efficiency and longevity [32]. Overcoming the system's power quality and guaranteeing the fuel cell system functions under an appropriate powerpoint were addressed in a study that used a super-twisting algorithm (STA) to determine the efficacy of robust high-order SMC [33]. In the PEMFC system, another author provided research comparing the effectiveness of first-order SMC and the STA in reducing chattering and increasing the system's lifetime under varying resistance loads [34]. STSM and the PI controller in an interleaved boost converter are compared concerning response time and the effect of overshoot and undershoot inhibition [35]. To make the FIBC more resistant to fluctuations in circuit parameters, researchers developed a switch fault diagnosis technique based on SMC [36]. A robust model predictive control (MPC) is demonstrated on a FIBC with different uncertainties [37]. A novel fault remedy was given in a study to address the problem of excessive input current ripple when a switch fails in a FIBC [38].

The purpose of this study is to use the PEMFC dynamic model and robust control in the DC/DC converter. The PEMFC system's MPP can be located with the aid of the STSM. The reference current estimator's job is to locate the MPP, and the values of the resulting currents will be used as the controller's reference current. This article shows how well the suggested controller holds up against variations in oxygen and hydrogen partial pressure, two fuel cell parameters that are prone to uncertainty. The IBC and FIBC system efficiencies will be compared to evaluate the efficiency of the findings. Following is a summary of this study's major contribution:

(1) A robust control and dynamic model of the PEMFC is implemented and incorporated with a FIBC.
(2) The performance of the PEMFC is considered during the construction of the STSM controller combined with the MPPT controller.
(3) The simulation validation is established under fuel cell variations to identify the system's efficiency which can help to achieve the SDG-7.

This study has been separated into the following parts. The PEMFC modeling is described in section II. The modeling of IBC and FIBC are discussed in Section III. The PEMFC system's control architecture is presented in Section IV. The findings and analysis of the project are presented in Section V. Section VI provides a summary of the study's conclusions.

2. Modeling of PEMFC

Fig. 1 demonstrates the PEMFC system's control design. Using the MATLAB/Simulink software, the efficiency of this control system is examined.

Fig. 2 illustrates a PEMFC, an electrochemical energy converter device that transforms chemical elements into electricity while producing heat and water.

Fig. 3 shows a PEMFC with two electrodes. The two electrodes are the anode and the cathode, an electrolyte membrane separating them. In the operation system, the fuels that used to generate electricity is the hydrogen and oxygen gas. The anode part of the fuel cell is responsible for splitting the incoming hydrogen atoms into electrons and protons. Electrons' motion is blocked, so they can't cross the electrolyte barrier, allowing only protons to pass through. As a result, electricity will be generated as electrons travel to the external circuit. Water and heat are produced as a byproduct when oxygen entering the cathode side reacts with electrons from the external circuit [39].

$$\begin{aligned} \text{Anode}: \ & 2H_2 \rightarrow 4H^+ + 4e^- \\ \text{Cathode}: \ & O_2 + 4H^+ + 4e^- \rightarrow 2H_2O \\ \text{Cell}: \ & 2H_2 + O_2 \rightarrow 2H_2O \end{aligned} \tag{1}$$

The PEMFC's mathematical model is given to explain the logic behind the system's design. Fuel cell efficiency can be affected by a number of variables, including temperature, supplied partial pressure, stack voltage, and load current. The IV and PV characteristic curves can be formed by applying the mathematical expression related to the variables of the fuel cell system. The IV and PV curve is presented under a single cell and operated at normal temperature and supplied pressure.

The overall output voltage of the fuel system is expressed as [40]:

$$V_{FC} = E_{cell} - V_{act} - V_{ohm} - V_{conc} \tag{2}$$

In which the V_{FC} is the fuel cell open circuit voltage, E_{cell} represents the reversible cell potential, and the rest represents the three losses in the system, respectively. In practice, as shown in Fig. 4, the PEM fuel cell potential value is less than the ideal theoretical potential due to the losses that occurred. The three main losses are the activation loss V_{act}, ohmic loss V_{ohm} and the concentration loss V_{conc} respectively.

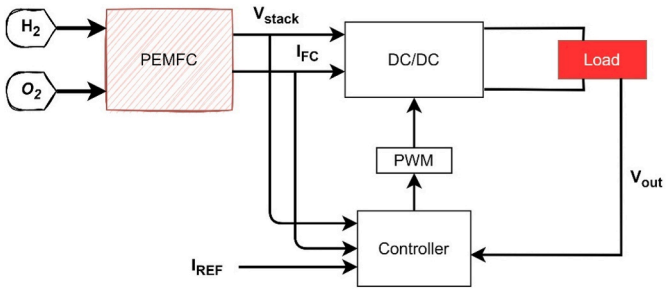

Fig. 1. Control design of PEM fuel cell.

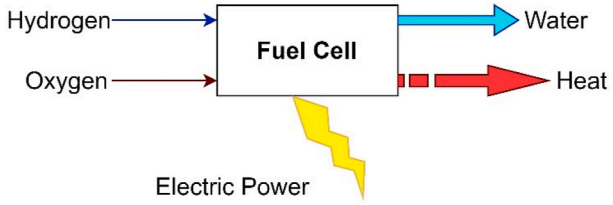

Fig. 2. Schematic representation of PEM fuel cell.

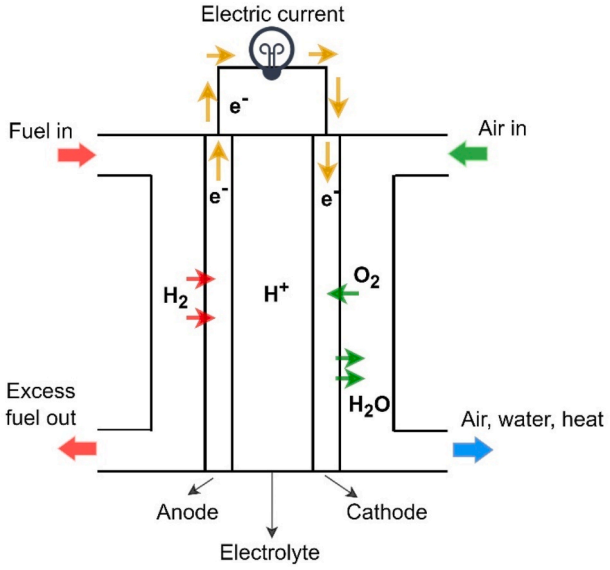

Fig. 3. PEM fuel cell operation diagram.

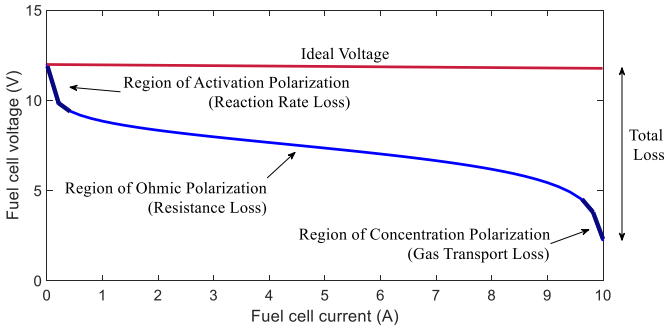

Fig. 4. Ideal and actual IV characteristics curve of PEMFC.

The reversible cell potential, E_{cell} is the electrical energy produced by the PEMFC and it is also the ideal output voltage. The E_{cell} theoretical expression is described as follows:

$$E_{cell} = 1.229 - 0.85 \times 10^{-3}(T - 298.15) + 4.3085 \times 10^{-5} \times T \ln(P_{H_2}) + 0.5 \ln(P_{O_2}) \tag{3}$$

where T is the cell operating temperature, P_{H2} and P_{O2} are the partial pressures of hydrogen and oxygen in the fuel cell's supplied in (atm).

The activation losses (V_{act}) are a type of loss that occurs when there is an interaction between the gasses, especially the oxygen gas. To calculate the activation overvoltage in the fuel cell, the equation is given as follows:

$$V_{act} = \varepsilon_1 + \varepsilon_2 T + \varepsilon_3 T \ln C_{O_2} + \varepsilon_4 T \ln I \tag{4}$$

where $\varepsilon_1 - \varepsilon_4$ are the parametric coefficients, CO_2 is the oxygen concentration that appears in the catalyst, and I represents the fuel cell load current. The oxygen concentration CO_2 is calculated by:

$$C_{O_2} = \frac{P_{O_2}}{5.08 \times 10^6 e^{\left(\frac{-498}{T}\right)}} \tag{5}$$

Due to the proton and electron transfer mechanism, the ohmic losses (V_{ohm}) are taken placed from the proton resistance R_m and the electron resistance R_c. The ohmic losses are expressed as:

$$V_{ohm} = I(R_c + R_m) \tag{6}$$

and

$$R_m = \frac{\rho_m l}{A} \tag{7}$$

where the ρ_m is the specific resistance of the membrane, A is the active area of the membrane, and l is the membrane thickness. The solution can be written as:

$$\rho_m = \frac{181.6\left[1 + 0.03\left(\frac{I}{A}\right) + 0.062\left(\frac{T}{303}\right)^2\left(\frac{I}{A}\right)^{2.5}\right]}{\left[\varphi - 0.634 - 3\left(\frac{I}{A}\right)e^{\left[\frac{4.18(T-303)}{T}\right]}\right]} \tag{8}$$

where φ is the water content of the membrane.

The concentration losses (V_{conc}) results from the drop of reaction gasses concentration during the reaction process. The equation of the concentration losses is presented as follows:

$$V_{conc} = B \ln\left(1 - \frac{J}{J_{max}}\right) \tag{9}$$

where B is the constant value based on the fuel cell type, J and J_{max} are respectively represent the current density and maximum current density. The following expression can be used to determine the current density J:

$$J = \frac{I}{A} \tag{10}$$

All of the above formulae can be used to compute the fuel cell stack. The fuel cell stack voltage equation is expressed as follows:

$$V_{stack} = N_{cell} V_{FC} \tag{11}$$

where N_{cell} represents the total amount of fuel cell cells. The following demonstrates the PEM fuel cell's power source:

$$P_{stack} = IV_{stack} \tag{12}$$

3. Modeling of dc-dc converters

A. Interleaved Boost Converter Model (IBC)

The interleaved boost converter (IBC) is a DC/DC converter with a multilevel of the standard boost converter. In Fig. 5(a), the topology of IBC is illustrated. This type of converter has advantages in ripple reduction and better fault-tolerant ability due to its interleaved structure. The figure clearly shows that the IBC has two pairs of inductors I_i $(i = 1, 2)$, diodes D_i $(i = 1, 2)$ and switches S_i $(i = 1, 2)$ together with one capacitor C and a load resistance R. The duty ratio's effect on the voltage at both the intake and output is shown as follows:

$$\frac{V_o}{V_{in}} = \frac{1}{1 - d(t)} \tag{13}$$

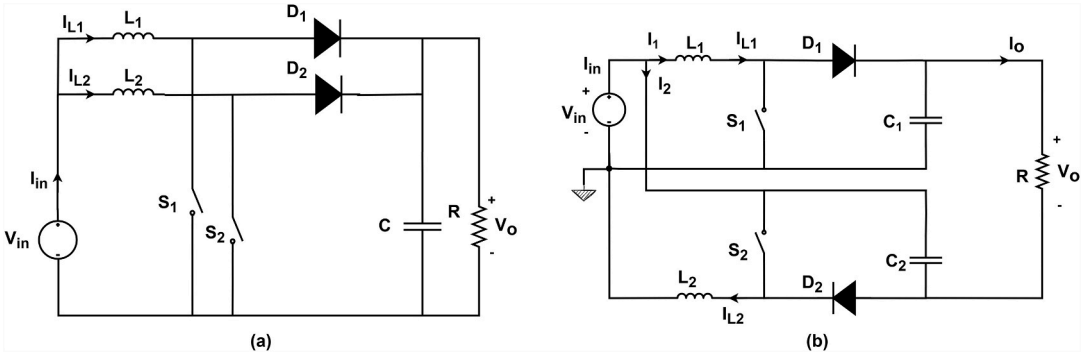

Fig. 5. (a) IBC topology, (b) FIBC topology.

where V_o and V_{in} are the output voltage and input voltage, respectively. The $d(t)$ represents the duty ratio.

For a two-phase IBC, there are two states for each switch: the open and close. By considering all working principles under the open and closed states, the mathematical expression of the IBC can be obtained. For example, when S_1 is closed and S_2 is opened, the equations of inductor and capacitor according to Kichhoff's law are expressed as follows:

$$\begin{aligned} L_1\frac{dI_{L1}(t)}{dt} &= +V_{in}(t) \\ L_2\frac{dI_{L2}(t)}{dt} &= -V_o(t) + V_{in}(t) \\ C\frac{dV_o(t)}{dt} &= I_{L2}(t) - \frac{V_o(t)}{R} \end{aligned} \tag{14}$$

An average model of the IBC's state space is computed for additional planning work. The average state-space model for this converter can be obtained by assuming that all converter stages have the same duty cycle. Following is a presentation of the typical state space model:

$$\begin{aligned} \frac{dI_{Li}}{dt} &= -\frac{1-d(t)}{L_i}V_o + \frac{1}{L_i}V_{in} \\ \frac{dV_o}{dt} &= \frac{1-d(t)}{C}\sum_{i=1}^{2} I_{Li} - \frac{1}{RC}V_o \end{aligned} \tag{15}$$

Understanding the ripple effect is important in this part since the current ripple is an important issue that will influence the lifespan of the fuel cell system. The current ripple ΔI_{in} of the IBC is expressed as:

$$\Delta I_{in} = \frac{V_o}{Lf_s d(t)(1-d(t))} \tag{16}$$

where f_s is the switching frequency.

The IBC contains two states of operation. Hence, the two states' differential stages of the duty ratio are combined and presented. The equations of the ΔI_{in} and ΔV_o are presented as follows:

$$\Delta I_{in} = \begin{cases} \dfrac{V_o}{f_s L}d(t)(1-d(t)) & 0 < d(t) < 0.5 \\ \dfrac{V_o}{f_s L}(d(t)-0.5)(2-2d(t)) & 0.5 < d(t) < 1 \end{cases} \tag{17}$$

and

$$\Delta V_o = \begin{cases} \dfrac{P_o}{f_s V_o C}\dfrac{d(t)(d(t)-0.5)}{d(t)-1} & 0 < d(t) < 0.5 \\ \dfrac{P_o}{f_s V_o C}(d(t)-0.5) & 0.5 < d(t) < 1 \end{cases} \tag{18}$$

B. Floating Interleaved Boost Converter Model (FIBC)

The floating interleaved boost converter (FIBC) can be formed as two boost converters combined with parallel input and series output, as shown in Fig. 5(b). From the figure, it showed that the topology of the FIBC has two capacitors C_i $(i = 1, 2)$, two inductors I_i $(i = 1, 2)$, two diodes D_i $(i = 1, 2)$, and two switches S_i $(i = 1, 2)$. V_{in} represents the voltage input, V_o as the output voltage and resistor R as the load resistance. The interleaved structure of the converter makes it beneficial in several aspects, such as it can provide a better fault-tolerant ability and better reduction in the ripple effect. The FIBC's high voltage gain capacity is complemented by the fact that it reduces voltage stress on the semiconductor. It's more efficient than a standard interleaved boost converter, allowing for the same voltage gain at a lower duty cycle [41].

Kirchhoff's voltage law is used to obtain the output voltage as follows:

$$V_o = V_{C1} + V_{C2} - V_{stack} \tag{19}$$

where V_{C1} and V_{C2} are the voltage across C_1 and C_2 respectively. The V_{stack} is the V_{in} of the fuel cell system.

The input source current is obtained by applying Kirchhoff's current law to the circuit. The equation is presented as follows:

$$I_L = I_1 + I_2 = I_{L1} + I_2 = I_{L1} + (I_{L2} - I_o) \tag{20}$$

where I_o is the output current at the load, I_{L1} and I_{L2} are the current flow across the inductor L_1 and inductor L_2 respectively.

To simplify the design process, the condition is given that the converter is symmetric between modules, it is assumed that

$$L_1 = L_2 = L, \;\; C_1 = C_2 = C, \;\; d_1(t) = d_2(t) = d(t) \tag{21}$$

where $d_i(t)$ $(i = 1, 2)$ is the duty ratio.

After all the losses are ignored, the converter voltage gain can be presented as follows:

$$\frac{V_o}{V_{stack}} = \frac{1+d(t)}{1-d(t)} \tag{22}$$

The proper inductor sizing is guaranteed by using the presented continuous conduction mode (CCM) operation. There are two operation modes in this converter. First, when the switch S_i $(i = 1, 2)$ is ON, the energy is stored in the inductor L_i and the capacitor C_i will be discharged through another capacitor and load. When the S_i $(i = 1, 2)$ is OFF, the inductor L_i and the energy source will charge the capacitor C_i through the diode D_i. The model of the FIBC is shown as follows [42]:

$$\frac{dI_{L1}}{dt} = \frac{1}{L_1}(V_{in} - (1-d_1(t))V_{C1})$$

$$= \frac{1}{2L}((d_1(t)+1)V_{in} + (d_1(t)-1)V_o)$$

$$\frac{dI_{L2}}{dt} = \frac{1}{L_2}(V_{in} - (1-d_2(t))V_{C2})$$

$$= \frac{1}{2L}((d_2(t)+1)V_{in} + (d_2(t)-1)V_o)$$

$$\frac{dV_{C1}}{dt} = \frac{1}{C_1}((1-d_1(t))I_{L1} - I_o)$$

$$= \frac{1}{C}((1-d_1(t))I_{L1} - I_o)$$

$$\frac{dV_{C2}}{dt} = \frac{1}{C_2}((1-d_2(t))I_{L2} - I_o)$$

$$= \frac{1}{C}((1-d_2(t))I_{L2} - I_o) \quad (23)$$

The inhibition of ripple effects ΔI_{in} plays an important role in extending the fuel cell stack lifespan. The current ripple is the difference between the stack current's highest and lowest values. The fuel cell stack current ripple is written as:

$$\Delta I_{in} = \frac{V_{in} d(t)}{f_s L} \quad (24)$$

where f_s represents the switching frequency.

Due to the structure of FIBC, a phase shift of π will occur between the switches and the input current ripple ΔI_{in} can be described as follows:

$$\Delta I_{in} = \begin{cases} \frac{V_o}{f_s L} \frac{d(t)(1-d(t))(1-2d(t))}{(1+d(t))^2} & 0 < d(t) < 0.5 \\ \frac{V_o}{f_s L} \frac{(1-d(t))^2(2d(t)-1)}{(1+d(t))^2} & 0.5 < d(t) < 1 \end{cases} \quad (25)$$

The peak-to-peak voltage ripple of the system is expressed as follows:

$$\Delta V_c = \frac{i_o d(t)}{f_s C} \quad (26)$$

where i_o is the average value of the load current I_o.

One of the advantages of FIBC is its ability to voltage and current stress reduction. Therefore, the voltage and current stresses of the converter are summarized and recorded in Table 1.

4. Implementation of the PEMFC control system

This part demonstrates the implementation of the PEMFC control system. The control design aims to ensure constant output results when applying the FIBC in a PEMFC system. The PEMFC is a non-linear system. Therefore, PI and PID controller is not suitable to use as a controller during the occurrence of disturbances and uncertainties. Thus, a robustness control, SMC is designed to control the PEMFC system. This research implements a STSM controller based on the MPPT technique. The robustness of the system is analyzed under fuel cell partial pressure variations. There are two steps in this control design. The first is to use the MPPT method with a reference current estimator (RCE) to determine the fuel cell system's peak power output. The maximum current values obtained in this way will be used as a reference for the fuel cell system. The second stage is to create a STSM controller that allows the current values to drift toward the reference current and reach the MPP extraction level regardless of the partial pressure variations of the fuel cell.

Table 1
Converter component stresses.

Component	Current stress	Voltage stress
Inductor	$\frac{I_{in}}{1+D}$	×
Capacitor	×	$\frac{V_o}{1+D}$
Diode	$\frac{I_{in}}{1+D}$	$\frac{V_o}{1+D}$
Switch	$\frac{I_{in}}{1+D}$	$\frac{V_o}{1+D}$

A. Reference Current Estimator (RCE)

The reference current estimator (RCE) is a type of MPPT method to determine the I_{max} which is the reference current I_{ref} under different operating conditions. PEMFC performance is sensitive to hydrogen and oxygen partial pressure that is provided. To study the effect of the hydrogen and oxygen variations in the fuel cell system, several tests are carried out and the maximum power P_{max}, and its corresponding maximum current I_{max} is recorded in Table 2. The recorded values will be used to generate a MPPT curve. The MPPT curve is built using the Matlab Curve Fitting Toolbox (CFT), as shown in Fig. 6.

As mentioned the collected data of P_{max} and I_{max} is imported into the CFT and will be tested under various types of fit categories to obtain the best-fit curve for the MPPT. The equation of the best-fit curve will be formed as follows:

$$I_{max} = \left(\frac{P_{max}}{a}\right)^{\frac{1}{b}} \quad (27)$$

where the coefficient values and the goodness of the fit are shown in Table 3.

The working principle of RCE is explained and shown in Fig. 7. By forming and observing several projections of the MPP curve (blue curve), the PEMFC system can reach its desired point, the maximum power of the system from its original operating point. In general, when the operating point P_{01} is with the I_{01}. The tracking control will start to project the P_{01} on the MPP curve which indirectly changes the I_{01} to I_{02} and at the same time, the operating power point will move to P_{02}. The same process will be repeated several times until the MPP of the system is reached which means when the MPP curve intersects with the P–I curve of the PEMFC system [43].

B. Super-twisting Sliding Mode Control (STSM)

Super-twisting sliding mode (STSM) is a 2-order SMC, which contains all the advantages of the conventional SMC and chattering reduction. It can generally maintain the system's robustness against uncertainties and disturbances and provide high accuracy in the system tracking process. The main feature of the STSM is that it does not require information about the time derivative since the design process only needs to know the sliding variable. This will make the controller's design process more straightforward and can be widely applied in many applications. In this research, the STSM is used as a controller to make sure the PEMFC operates at an efficient powerpoint. The STSM controller will generate a control signal $u(t)$ for the switch S_i $(i = 1, 2)$ after obtaining the sliding surface $e = I_L - I_{ref}$. The control law $u(t)$ is expressed as [43]:

$$u(t) = u_1(t) + u_2(t) \quad (28)$$

with

$$\begin{aligned} u_1(t) &= -k_1 \int \text{sign}(s) dt \\ u_2(t) &= -k_2 |s|^{\rho} \text{sign}(s) \end{aligned} \quad (29)$$

where k_1, k_2 and $\rho \in (0, 1/2]$ are the parameters decided by the designer. The necessary circumstances for the convergence of the sliding surface can be derived [44]:

Table 2
P_{max} and I_{max} values obtained from the PEMFC model.

	P_{H2}=0.02 atm, P_{O2}=0.04 atm	P_{H2}=0.2 atm, P_{O2}=0.4 atm	P_{H2}=2 atm, P_{O2}=4 atm
P_{max}	39.42	49.78	60.45
I_{max}	8.2	8.4	8.6

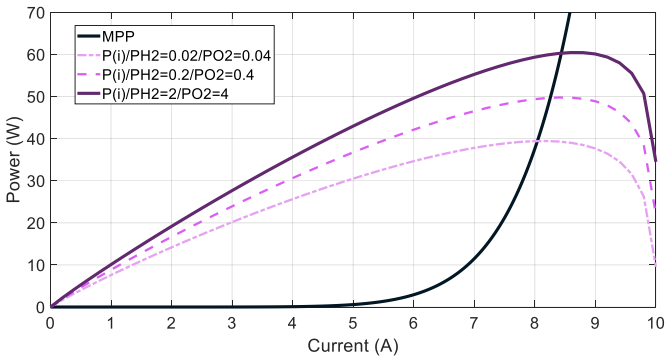

Fig. 6. MPPT curve.

Table 3
The goodness of fit and coefficient values of the fitting function.

The goodness of the fit			
SSE: 0.4574	R-square: 0.9979	Adjusted R-square: 0.9959	RMSE: 0.6763
Coefficients			
a = 3.069e-07	b = 8.878		

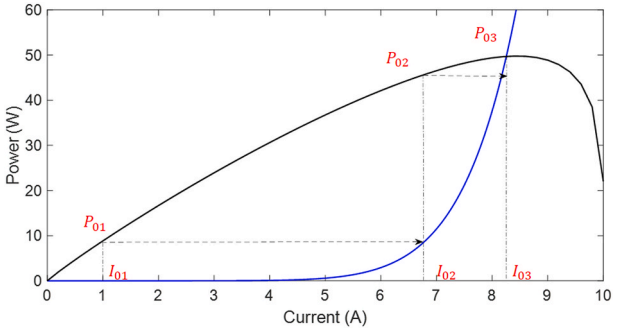

Fig. 7. RCE operating principle.

$$k_1 > \frac{\phi}{\Gamma_m}$$
$$k_2 > \frac{2}{\Gamma_m^2}\frac{(\Gamma_m\alpha+\phi)^2}{\Gamma_m\alpha-\phi} \tag{30}$$

The STSM's final control rule is derived from the descriptions above. Fig. 8 depicts the phase trajectory of the super-twisting sliding mode control.

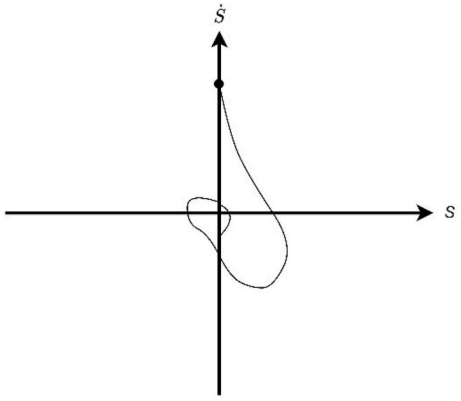

Fig. 8. Phase trajectory of STSM.

5. Results and discussions

MATLAB/Simulink is used for modeling purposes to test the efficiency and stability of the system. Table 4 displays the PEMFC model parameters and Table 5 displays the IBC and FIBC parameters.

A. PEM fuel cell model

Examining the PEMFC system's efficiency is a top priority. It is tested under various operating circumstances. The performance of the fuel cell device is shown in Fig. 9 for a range of operating temperatures from 298.15 K to 373.15 K, with the hydrogen partial pressure set at 0.2 atm and the oxygen partial pressure set at 0.4 atm. According to the graph, the fuel cell's output voltage increases as the working temperature rises.

The fuel cell's operating partial pressure also affects its efficiency. The polarization curve at various operating conditions of hydrogen partial pressures (shown in Fig. 10) ranges from 0.02 to 2 atm, while the oxygen partial pressure ranges from 0.04 to 4 atm. To generate the characteristics curves, the temperature of the fuel cell is set at 298.15 K. The results showed that when the supplied partial pressure is high, the output voltage produced by the fuel cell is also high. Therefore, the results validate that the efficiency of the fuel cell system is improved when the operating condition of temperature and partial pressure is increased.

B. Control Results

At $t = 1$ s and $t = 2$ s, the hydrogen and oxygen partial pressures are monitored to determine the system's activity (see Fig. 10). The initial partial pressures of hydrogen and oxygen are 0.02 atm and 0.04 atm, respectively. Both the hydrogen and oxygen partial pressures are adjusted to a range of 0.02–0.2 atm and 0.04–0.4 atm, respectively, at $t = 1$ s. At time $t = 2$ s, the provided hydrogen and oxygen partial pressures will change from 0.2 to 2 atm and 0.4–4 atm, respectively.

The PEMFC device and the converter designs for the IBC and FIBC are verified further in a simulation setting using MATLAB/Simulink. In Fig. 10, the outcomes of two scenarios where the partial pressure is changed: one at $t = 1$ s and another at $t = 2$ s. Fig. 11 shows the results of the fuel-cell-controlled IBC. To test how well the system can function to provide efficient power despite variations in hydrogen and oxygen partial pressure, a simulation is run using the controller of the MPPT method based on STSM. Fig. 11(a) and (b) show the efficiency of the fuel cell voltage and current as well as the output voltage and current at different fuel cell partial pressures. Fig. 11(c) and (d) demonstrate the fuel cell system's maximum power point and its output power, respectively. Fig. 12 presents the results of FIBC under the same conditions as IBC for comparison.

According to the results, both of the converters can retain the

Table 4
PEMFC parameter values.

Symbol	Value	Unit
E_o	1.229	V
R	83.143	$Jmol^{-1}K^{-1}$
F	96485.309	$Cmol^{-1}$
T	298.15	K
A	162	cm^2
ψ	23	
l	175×10^{-6}	cm
B	0.1	V
R_c	0.0003	
J_{max}	0.062	Acm^{-1}
N_{cell}	10	
ε_1	0.9514	V
ε_2	−0.00312	V/K
ε_3	-7.4×10^{-5}	V/K
ε_4	1.87×10^{-4}	V/K

Table 5
Circuit parameter of the converters.

Symbol	Value	Unit
L	69	mH
R	20	Ω
C	1500	μF
f_s	5	kHz

system's stability and ensure the system tracks down the maximum power point. In a particular simulation, the two types of converter function differently. Table 6 provides a list of results for the quantitative performance of the output voltage. The following conclusions could be obtained from Table 6: (i) The voltage ripples are significantly reduced by using FIBC when partial pressure changes; (ii) IBC has better inhibition in the voltage undershoot; (iii) FIBC has a faster response time than the IBC. Overall, it can be said that the FIBC has a close effect on the IBC in voltage undershoot inhibition when the fuel cell partial pressure varies and has significant advantages in disturbance rejection.

According to Table 7, both the IBC and the FIBC have satisfactory ripple current decreases in fuel cells in response to hydrogen and oxygen partial pressure changes. The chattering impact of the SMC is the root cause of this problem. The STSM controller, as a higher-order sliding mode, can minimize the chattering effect in some circumstances. However, it cannot be completely removed. When compared to the IBC, the FIBC can provide better performance in reducing the fuel cell current overshoot under the condition of fuel cell partial pressure variations. However, there isn't a clear constraint in any research or effort regarding the present overshoot and undershoot; it is still important to ensure the values are kept as low as possible to retain the fuel cell operating performance. This is because large overshoot and undershoot will provide the possibility of false protection in the fuel cell system when the current surpasses the maximum current protection value in a short period of time.

The FIBC shows that it is a better selection to work with the PEMFC system because it combines the capabilities of two converters regarding fuel cell current and output voltage. Strong robustness is demonstrated by the FIBC, particularly regarding the response time and ripple effect inhibition effectiveness. Although there are some shortcomings, such as the output voltage overshoot reduction, when compared to the IBC, the overall performance is still satisfactory and meets the requirements of the fuel cell system.

6. Conclusion

This research discusses and develops a comprehensive mathematical model of the PEMFC incorporated with DC/DC converters. Additionally, a controller is designed for maximum power tracking of the PEMFC system. MATLAB/Simulink is used to build and test the complete system driven by the MPPT technique based on the STSM controller. The IV and PV characteristics curve examines the fuel cell's performance at different operating conditions. The results are proven through simulation that the MPPT method based on the STSM controller provides satisfactory tracking performance with respect to the maximum power point. With the obtained maximum power point, the STSM controller can select the corresponding reference current values to reach the required maximum power point. To test the system's robustness, the proposed controller's performance is a test subject to the uncertainties of the PEMFC parameters. Furthermore, the controller designs are carried out with two different types of converters: the IBC and FIBC. It is clearly shown that both converters can maintain the system's stability when working with the proposed controller. However, FIBC showed strong robustness under fuel cell partial pressure variations in terms of the ripple inhibition effect, response time, and current overshoot compared to the IBC. Using the proposed converter with the proper controller on the PEMFC system ensures the system's efficiency and makes it become a

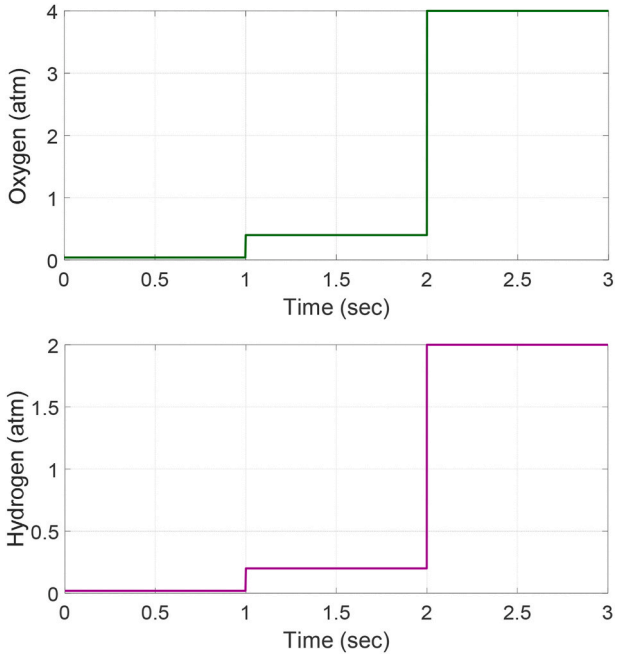

Fig. 10. Oxygen and hydrogen partial pressure variations.

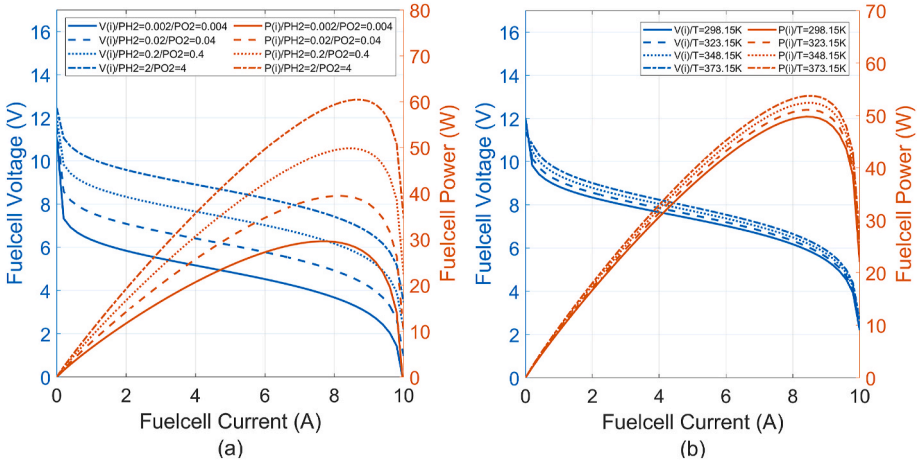

Fig. 9. (a) PV and IV curve at different operating partial pressures, (b) PV and IV curve at different operating temperature.

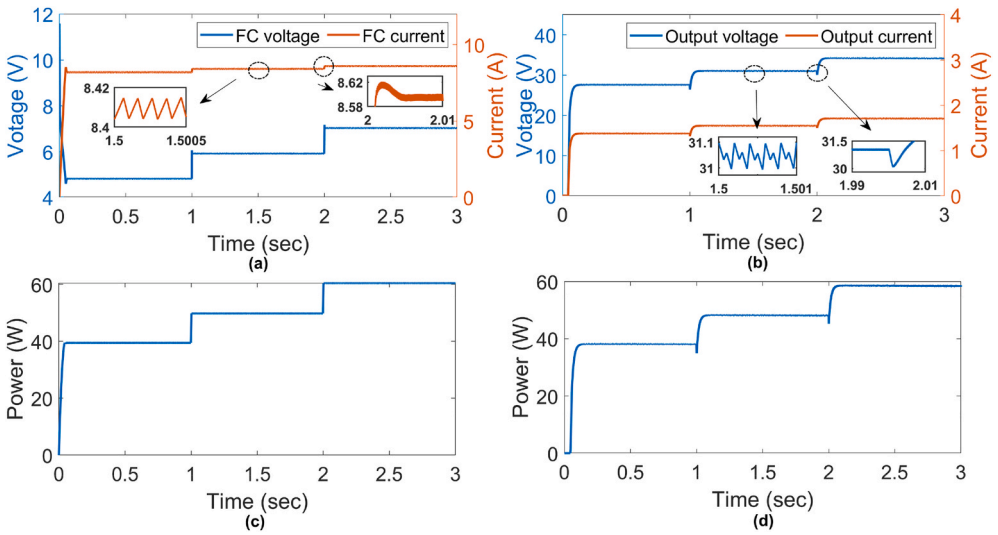

Fig. 11. Simulation results with IBC controller. (a) Fuel cell results, (b) output results, (c) input power result, (d) output power result.

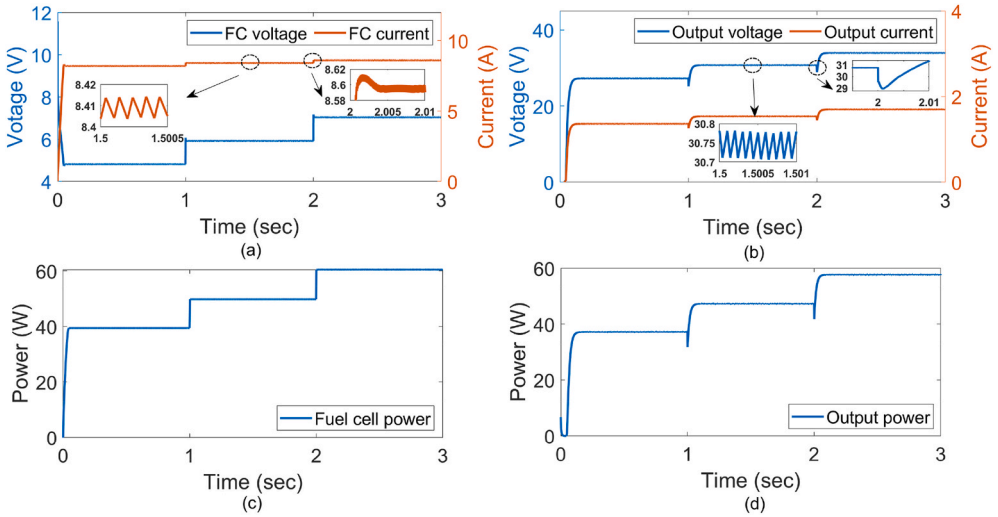

Fig. 12. Simulation results with FIBC controller. (a) Fuel cell results, (b) output results, (c) input power result, (d) output power result.

Table 6
Quantitative performance of the output voltage.

Converter	Response time (ms)	Voltage undershoot (V)
IBC	69.485	0.99
FIBC	67.192	1.946

Table 7
Quantitative performance of the fc current ripple.

Converter	Current ripple (mA)	Current overshoot (mA)
IBC	11.73	25.35
FIBC	11.17	18.92

system that can be used to achieve the SDG-7 goals.

CRediT authorship contribution statement

Jie Ying Tan: Writing – original draft, Software, Methodology, Data curation. **Raja Mohd Taufika Raja Ismail:** Writing – review & editing, Supervision, Funding acquisition, Conceptualization. **Mohd Shawal Jadin:** Writing – review & editing, Supervision.

Declaration of competing interest

The authors declare that they have no known competing financial interests or personal relationships that could have appeared to influence the work reported in this paper.

Data availability

The data that has been used is confidential.

Acknowledgment

This research is supported by the Ministry of Education, Malaysia (FRGS/1/2021/TK0/UMP/02/71) and Universiti Malaysia Pahang Al-Sultan Abdullah, Malaysia under grant number RDU210128.

References

[1] A.A. Youssef, S. Barakat, E. Tag-Eldin, M.M. Samy, Islanded green energy system optimal analysis using PV, wind, biomass, and battery resources with various

economic criteria, Results in Engineering 19 (Sep. 2023) 101321, https://doi.org/10.1016/J.RINENG.2023.101321.
[2] H. Chojaa, et al., Robust control of DFIG-based WECS integrating an energy storage system with intelligent MPPT under a real wind profile, IEEE Access 11 (2023) 90065–90083, https://doi.org/10.1109/ACCESS.2023.3306722.
[3] L. Schirone, F. Pellitteri, Energy policies and sustainable management of energy sources, Sustainability 9 (12) (Dec. 2017) 2321, https://doi.org/10.3390/su9122321.
[4] M. Yessef, et al., Improving the maximum power extraction from wind turbines using a second-generation CRONE controller, Energies 15 (10) (May 2022) 3644, https://doi.org/10.3390/en15103644.
[5] S. Boulmrharj, M. Khaidar, M. Bakhouya, R. Ouladsine, M. Siniti, K. Zine-dine, Performance assessment of a hybrid system with hydrogen storage and fuel cell for cogeneration in buildings, Sustainability 12 (12) (Jun. 2020) 4832, https://doi.org/10.3390/su12124832.
[6] A. Loulijat, et al., Enhancement of LVRT ability of DFIG wind turbine by an improved protection scheme with a modified advanced nonlinear control loop, Processes 11 (5) (May 2023) 1417, https://doi.org/10.3390/pr11051417.
[7] A. Farooq, W. Alhalabi, Evaluation of hydrogen fuel cell-based systematic vehicular application to promote the green economy using LabVIEW, Results in Engineering 20 (Dec. 2023) 101607, https://doi.org/10.1016/j.rineng.2023.101607.
[8] U. Sarma, S. Ganguly, Determination of the component sizing for the PEM fuel cell-battery hybrid energy system for locomotive application using particle swarm optimization, J. Energy Storage 19 (Oct. 2018) 247–259, https://doi.org/10.1016/j.est.2018.08.008.
[9] S.A. Niknam, M. Mortazavi, A.D. Santamaria, Signature analysis of two-phase flow pressure drop in proton exchange membrane fuel cell flow channels, Results in Engineering 5 (Mar. 2020) 100071, https://doi.org/10.1016/j.rineng.2019.100071.
[10] S. Wang, S.P. Jiang, Prospects of fuel cell technologies, Natl. Sci. Rev. 4 (2) (Mar. 2017) 163–166, https://doi.org/10.1093/nsr/nww099.
[11] M. Aravindan, G. Praveen Kumar, Hydrogen towards sustainable transition: a review of production, economic, environmental impact and scaling factors, Results in Engineering 20 (Dec. 2023) 101456, https://doi.org/10.1016/j.rineng.2023.101456.
[12] X. He, et al., Well-to-wheels emissions, costs, and feedstock potentials for light-duty hydrogen fuel cell vehicles in China in 2017 and 2030, Renew. Sustain. Energy Rev. 137 (Mar. 2021) 110477, https://doi.org/10.1016/j.rser.2020.110477.
[13] P.M. Falcone, M. Hiete, A. Sapio, Hydrogen economy and sustainable development goals: review and policy insights, Curr. Opin. Green Sustainable Chem. 31 (2021), https://doi.org/10.1016/j.cogsc.2021.100506.
[14] K. Martins, J.G. Carton, Prospective roles for green hydrogen as part of Ireland's decarbonisation strategy, Results in Engineering 18 (Jun. 2023) 101030, https://doi.org/10.1016/j.rineng.2023.101030.
[15] Q. Hassan, A.Z. Sameen, H.M. Salman, M. Jaszczur, M. Al-Hitmi, M. Alghoul, Energy futures and green hydrogen production: is Saudi Arabia trend? Results in Engineering 18 (Jun. 2023) 101165 https://doi.org/10.1016/J.RINENG.2023.101165.
[16] H. Mishra, S. Ray, T.V. Dixit, Design of double loop CDM controllers for proton exchange membrane fuel cell fed DC-DC boost converter under wide source and load variations, Int. J. Control Autom. Syst. 19 (5) (2021) 1873–1881, https://doi.org/10.1007/s12555-020-0237-8.
[17] M. Derbeli, O. Barambones, M.Y. Silaa, C. Napole, Real-time implementation of a new MPPT control method for a DC-DC boost converter used in a PEM fuel cell power system, Actuators 9 (4) (2020) 1–22, https://doi.org/10.3390/act9040105.
[18] A. Harrag, Novel neural network single sensor MPPT for proton exchange membrane fuel cell, J. N. Mater. Electrochem. Syst. 24 (1) (2021) 43–48, https://doi.org/10.14447/jnmes.v24i1.a08.
[19] M. Zunita, A. Raizki, R. Aditya, I.G. Wenten, Proton exchange polyionic liquid-based membrane fuel cell applications, Results in Engineering 16 (Dec. 2022) 100653, https://doi.org/10.1016/j.rineng.2022.100653.
[20] M. Ma, X. Liu, K.Y. Lee, Maximum power point tracking and voltage regulation of two-stage grid-tied PV system based on model predictive control, Energies 13 (6) (2020), https://doi.org/10.3390/en13061304.
[21] M. Yessef, B. Bossoufi, M. Taoussi, A. Lagrioui, H. Chojaa, Overview of control strategies for wind turbines: ANNC, FLC, SMC, BSC, and PI controllers, Wind Eng. 46 (6) (Jun. 2022) 1820–1837, https://doi.org/10.1177/0309524X221109512.
[22] H. Chojaa, et al., Advanced control techniques for doubly-fed induction generators based wind energy conversion systems, in: 2022 Global Energy Conference (GEC), 2022, pp. 282–287, https://doi.org/10.1109/GEC55014.2022.9987088.
[23] E.M. Barhoumi, I. Ben Belgacem, A. Khiareddine, M. Zghaibeh, I. Tlili, A neural network-based four phases interleaved boost converter for fuel cell system applications, Energies 11 (12) (2018) 1–18, https://doi.org/10.3390/en11123423.
[24] R.A. Soumana, M.J. Saulo, C.M. Muriithi, New control strategy for multifunctional grid-connected photovoltaic systems, Results in Engineering 14 (Jun. 2022) 100422, https://doi.org/10.1016/J.RINENG.2022.100422.
[25] Q. Li, et al., An improved floating interleaved boost converter with the zero-ripple input current for fuel cell applications, IEEE Trans. Energy Convers. 34 (4) (2019) 2168–2179, https://doi.org/10.1109/TEC.2019.2936416.
[26] K. Mammar, F. Saadaoui, S. Laribi, Design of a PEM fuel cell model for flooding and drying diagnosis using fuzzy logic clustering, Renewable Energy Focus 30 (September) (2019) 123–130, https://doi.org/10.1016/j.ref.2019.06.001.
[27] K. Benaggoune, M. Yue, S. Jemei, N. Zerhouni, A data-driven method for multi-step-ahead prediction and long-term prognostics of proton exchange membrane fuel cell, Appl. Energy 313 (September 2021) (2022) 118835, https://doi.org/10.1016/j.apenergy.2022.118835.
[28] D.N. Luta, A.K. Raji, Fuzzy rule-based and particle swarm optimisation MPPT techniques for a fuel cell stack, Energies 12 (5) (2019), https://doi.org/10.3390/en12050936.
[29] Z. Tian, Z. Lyu, J. Yuan, C. Wang, UDE-based sliding mode control of DC–DC power converters with uncertainties, Control Eng. Pract. 83 (September 2018) (2019) 116–128, https://doi.org/10.1016/j.conengprac.2018.10.019.
[30] U. Javaid, A. Mehmood, A. Arshad, F. Imtiaz, J. Iqbal, Operational efficiency improvement of PEM fuel cell - a sliding mode based modern control approach, IEEE Access 8 (2020) 95823–95831, https://doi.org/10.1109/ACCESS.2020.2995895.
[31] K. Sankar, G. Saravanakumar, A.K. Jana, Nonlinear multivariable control of an integrated PEM fuel cell system with a DC-DC boost converter, Chem. Eng. Res. Des. 167 (2021) 141–156, https://doi.org/10.1016/j.cherd.2021.01.011.
[32] A. Dali, S. Abdelmalek, A. Bakdi, M. Bettayeb, A novel effective nonlinear state observer based robust nonlinear sliding mode controller for a 6 kW Proton Exchange Membrane Fuel Cell voltage regulation, Sustain. Energy Technol. Assessments 44 (April 2020) (2021), https://doi.org/10.1016/j.seta.2021.100996.
[33] M. Derbeli, O. Barambones, M. Farhat, J.A. Ramos-Hernanz, L. Sbita, Robust high order sliding mode control for performance improvement of PEM fuel cell power systems, Int. J. Hydrogen Energy 45 (53) (2020) 29222–29234, https://doi.org/10.1016/j.ijhydene.2020.07.172.
[34] M. Derbeli, O. Barambones, J.A. Ramos-Hernanz, L. Sbita, Real-time implementation of a super twisting algorithm for PEM fuel cell power system, Energies 12 (9) (2019) 1–20, https://doi.org/10.3390/en12091594.
[35] X. Hao, I. Salhi, S. Laghrouche, Y. Ait-Amirat, A. Djerdir, Robust control of four-phase interleaved boost converter by considering the performance of PEM fuel cell current, Int. J. Hydrogen Energy 46 (78) (2021) 38827–38840, https://doi.org/10.1016/j.ijhydene.2021.09.132.
[36] S. Zhuo, L. Xu, A. Gaillard, Y. Huangfu, D. Paire, F. Gao, Robust open-circuit fault diagnosis of multi-phase floating interleaved DC-DC boost converter based on sliding mode observer, IEEE Transactions on Transportation Electrification 5 (3) (2019) 638–649, https://doi.org/10.1109/TTE.2019.2921849.
[37] H. Sartipizadeh, F. Harirchi, M. Babakmehr, P. Dehghanian, Robust model predictive control of DC-DC floating interleaved boost converter with multiple uncertainties, IEEE Trans. Energy Convers. 36 (2) (2021) 1403–1412, https://doi.org/10.1109/TEC.2021.3058524.
[38] S. Zhuo, A. Gaillard, Q. Li, R. Ma, D. Paire, F. Gao, Current ripple optimization of four-phase floating interleaved DC-DC boost converter under switch fault, IEEE Trans. Ind. Appl. 56 (4) (2020) 4214–4224, https://doi.org/10.1109/TIA.2020.2986178.
[39] M.Y. Silaa, M. Derbeli, O. Barambones, A. Cheknane, Design and implementation of high order sliding mode control for PEMFC power system, Energies 13 (17) (2020) 1–15, https://doi.org/10.3390/en13174317.
[40] M.Y. Silaa, M. Derbeli, O. Barambones, C. Napole, A. Cheknane, J.M.G. de Durana, An efficient and robust current control for polymer electrolyte membrane fuel cell power system, Sustainability 13 (4) (2021) 1–18, https://doi.org/10.3390/su13042360.
[41] A. Farooq, Z. Malik, D. Qu, Z. Sun, G. Chen, A three-phase interleaved floating output boost converter, Adv. Mater. Sci. Eng. 2015 (2015), https://doi.org/10.1155/2015/409674.
[42] Y. Huangfu, S. Zhuo, F. Chen, S. Pang, D. Zhao, F. Gao, Robust voltage control of floating interleaved boost converter for fuel cell systems, IEEE Trans. Ind. Appl. 54 (1) (2018) 665–674, https://doi.org/10.1109/ETI4.051663.2021.9619445.
[43] A. Souissi, Adaptive sliding mode control of a PEM fuel cell system based on the super twisting algorithm, Energy Rep. 7 (Nov. 2021) 3390–3399, https://doi.org/10.1016/j.egyr.2021.05.069.
[44] S.V. Emel'yanov, S.K. Korovin, A. Levant, High-order sliding modes in control systems, Comput. Math. Model. 7 (3) (1996) 294–318, https://doi.org/10.1007/BF01128162.